Synthesis of Low Density Poly(ethylene) Using Nickel Iminophosphonamide Complexes

Russell A. Stapleton,[†] Jianfang Chai,[†] Anuttra Nuanthanom,[‡] Zygmunt Flisak,[§,⊥] Marcio Nele,[∥] Tom Ziegler,[§] Peter L. Rinaldi,[‡] Joao B. P. Soares,[#] and Scott Collins*[,‡]

Department of Polymer Science, The University of Akron, Akron, Ohio 44325-3909, Department of Chemistry, The University of Akron, Akron, Ohio 44325-3611, Department of Chemistry, The University of Calgary, Calgary, AB T2V 2R3, Canada, Institute of Chemistry, University of Opole, Oleska 48, 45-052 Opole, Poland, Escola de Química, Universidade Federal do Rio de Janeiro, Cidade Universitária, Rio de Janeiro, 68502, 21949-900 RJ, Brazil, and Department of Chemical Engineering, The University of Waterloo, Waterloo, ON N2L 3G1, Canada

Received October 9, 2006; Revised Manuscript Received January 8, 2007

ABSTRACT: Ethylene polymerization using a catalyst derived from the reaction of the phosphorane $(Me_3Si)_2NP(=NSiMe_3)_2$ (**1**) with either $Ni(COD)_2$ or bis(π-allyl)Ni complexes affords branched poly(ethylene) (PE) of variable MW (10^3-10^6) depending on conditions. The branched PE of high MW is semicrystalline with $T_m < 100$ °C. High field ^{13}C NMR spectra reveal the presence of methyl branches (ca. 10−15 per 1000 C atoms), branches longer than six C atoms (15−20 per 1000 C atoms) and trace levels of ethyl, propyl, *n*-butyl, and *sec*-butyl branches (total <2 per 1000 C atoms). The branching distribution changes modestly in response to changes in ethylene pressure in a manner consistent with a chain-walking mechanism. Analysis of high MW polymers by GPC-light scattering reveals the presence of sparse long-chain branching ($g^M = 0.78-0.93$ with <1 long-chain branch per molecule); the branched PE formed is thus similar to low-density PE. Addition of α-olefin during polymerization leads to enhanced activity but is accompanied by chain transfer. The only evidence of α-olefin incorporation is at the chain-ends in the case of 4-methylpentene, and there is little change to the branching distribution in the presence of α-olefin. A sterically hindered nickel iminophosphonamide (PN_2) complex $(Me_3Si)_2NP(Me)(NSiMe_3)_2NiPh(PPh_3)$ (**2**) was prepared and characterized by X-ray crystallography. This complex oligomerizes ethylene to branched material with a microstructure very similar to that observed using the catalysts derived from phosphorane **1** and $Ni(COD)_2$ or $(\pi\text{-allyl})_2Ni$. DFT modeling of the active catalyst, coupled with stochastic simulation of chain growth, reveals that a chain-walking vs insertion mechanism can account for the short-chain branching distributions observed. Kinetic modeling of the observed branching distribution can account for relative intensity of the short branches ($\leq C_5$) as well as those of the longer branches. However, in order to fit the intensity of the Hx^+ branches, one of the key parameters in the model, the probability of chain-walking for higher secondary Ni−R groups, converges to a value ∼ 1. This finding is not anticipated by the DFT results and suggests that the longer branches present in these materials do not form by a chain-walking vs insertion mechanism.

Introduction

There is considerable interest in the synthesis of branched poly(ethylene) (PE) using transition metal catalysts.[1] High density and linear low-density PE, both with sparse long-chain branching, typically <1 1ong-chain branch (LCB) per 1000 C atoms, are produced using *ansa*-metallocene and constrained geometry catalysts in solution, slurry or even gas-phase processes.[2] The mechanism of long-chain branch formation in these materials primarily involves macromonomer incorporation,[3] a process which is facilitated by the "open" coordination sphere about the metal in these kinds of catalysts.

On the other hand, using α-diimine and related catalysts of Ni and Pd, branched PE is formed from ethylene by a chain-walking vs insertion mechanism.[4] Depending on the ratio of the rates of these two competing processes, materials that have controllable levels of short-chain branching (e.g., 0−100 Me groups/1000 C atoms), depending on ethylene pressure, or even hyperbranched materials with dendritic architecture[5] are available when the catalyst is capable of "walking" past a branch point at a rate that is much faster than insertion.

The occurrence of long chain branches (LCB) in such materials, as occur in low-density PE,[6] has often been postulated from the branching distributions of these materials, based on the intensity of the signal due to branches ≥6 carbon atoms in the ^{13}C NMR spectrum (Hx^+).[7] However, there has been limited study of the rheologicial or other properties of these materials which are most sensitive to LCB.[5a−c] The evidence for LCB formation is strongest for materials prepared using Pd diimine catalysts while in the case of the more active Ni-catalysts, as far as we are aware, there is no conclusive evidence of LCB in the materials prepared under a range of conditions.

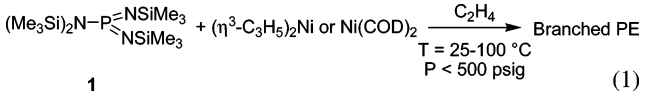

(1)

It is therefore of interest to note that the *first* synthesis of branched PE from ethylene monomer using a transition metal catalyst, reported by Keim and co-workers nearly 25 years ago, was said to provide a material resembling *low density* PE in its properties.[8] The catalyst was derived from reaction of phos-

* Corresponding author. E-mail: collins@uakron.edu.
[†] Department of Polymer Science, The University of Akron.
[‡] Department of Chemistry, The University of Akron.
[§] Department of Chemistry, The University of Calgary.
[⊥] Institute of Chemistry, University of Opole.
[∥] Escola de Química, Universidade Federal do Rio de Janeiro.
[#] Department of Chemical Engineering, The University of Waterloo.

10.1021/ma062332f CCC: $37.00 © 2007 American Chemical Society
Published on Web 03/31/2007

phorane **1** with either $Ni(COD)_2$ or $Ni(\eta^3\text{-}C_3H_6)_2$ in the presence of ethylene (eq 1).

The group of Fink has shown that these formulations are competent for the chain-straightening oligomerization of α-olefins at low *T* and have postulated that this occurs via a chain-walking mechanism.[9] Subsequent work from the group of Yano in Japan have revealed that these catalyst formulations produce poly(ethylene) with Me and Hx^+ branching as revealed by ^{13}C NMR analysis.[10] Further, the hydrodynamic volume of these polymers in solution was reduced compared with unbranched materials ($g' = [\eta]_{br}/[\eta]_{lin} = 0.6-0.8$). It was quite surprising to us that branches of intermediate length between Me and Hx^+ were not detected in the ^{13}C NMR spectra of these materials[10] while the total branching levels (<30 Me groups/1000 C atoms) were reduced from those typically seen with α-diimine catalysts and Pd catalysts in particular.

As we recently reported, the active catalyst involved in these polymerization processes is an alkylnickel iminophosphonamide (PN_2) complex, $PN_2Ni(L)R$ ($L = H_2C{=}CH_2$) formed in situ from the phosphorane and either the Ni(0) or Ni(II) precursor.[11] This was verified by independent synthesis of such a complex and demonstrating that it forms branched polymer with a similar microstructure to that produced using the Keim formulations. Unfortunately, the complex prepared [$Ph_2P(NSiMe_3)_2Ni(PPh_3)$-Ph] only furnished oligomers under the conditions investigated and so the issue of how LCB arose in these materials remained an open question.

In addition, it was unclear that the unusual branching distribution could be accounted for via a chain-walking vs insertion mechanism. For example, stochastic simulations of chain growth using kinetic modeling approaches for Ni diimine catalysts have failed to indicate formation of LCB by a chain-walking vs insertion mechanism.[12] In essence, once a catalyst has migrated a few carbon atoms down the chain (or past a branch point), it was assumed that it is equally probable for the metal to walk in either direction. Thus, the chain-walking process becomes a true random-walk and it is expected that formation of a long branch via such a process is improbable.

On the other hand, DFT calculations when combined with stochastic simulation, have indicated the formation of structures with LCB provided insertion into 1° Ni−R is much more favorable than insertion into 2° Ni−R and chain-walking is more rapid than insertion.[13] However, in this work, explicit inclusion of (different) chain-walking barriers was not considered nor was it evident whether walking backward was as probable as walking forward. One expects that LCB could only form in such materials if there is a significant difference in insertion barriers, that chain-walking is much faster than insertion and that chain-walking in the forward direction is favored over the reverse process.

In this paper we report the results of additional polymerization studies using the Keim catalysts, characterization of the materials formed by high field ^{13}C NMR spectroscopy, and GPC-light scattering which definitely reveals the presence of sparse LCB in these materials. We also summarize the results of some DFT calculations on models for the active catalyst and stochastic simulation of chain growth which are able to mimic the short-chain branching distribution. Finally, we briefly summarize the results of modeling of the branched microstructure, using a simplified kinetic model derived earlier.[12]

Results and Discussion

Ethylene Polymerization using Phosphorane 1 and Ni(COD)$_2$ or bis(π-allyl)Ni Complexes. Combining either the Ni(0) or Ni(II) precursor with phosphorane **1** in the presence of ethylene leads to slow ethylene consumption even at mM concentrations of Ni in toluene. In our hands, the combination of bis(π-allyl)Ni and phosphorane **1** was inactive at 70 °C and 450 psig, while use of $Ni(COD)_2$ at 60 °C and 30 psig, in the presence of 1-hexene (1-Hx), afforded a small amount ($A \sim 12$ kg PE/mol Ni × h) of a waxy material of low MW. Consequently, most of the systematic experiments were conducted at room temperature. However, the stability of these catalyst formulations is not high, even under these conditions, as revealed by the flow profile depicted in Figure 1.

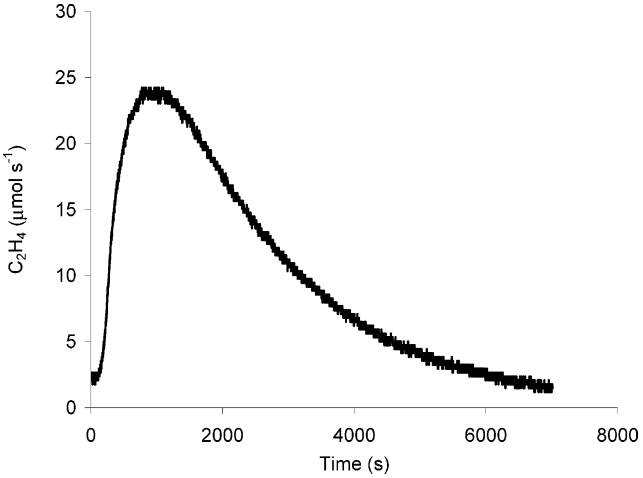

Figure 1. Ethylene flow vs time for a polymerization initiated by phosphorane **1** and $Ni(COD)_2$ in the presence of 1-hexene. For conditions, see Table 1, entry 5.

The most active formulation is that derived from the Ni(0) precursor and phosphorane **1** (Table 1, entries 1−6). As expected from the patent literature, addition of either 1-Hx or 4-methylpentene (4-MP) leads to enhanced activity although with a significant reduction in MW. In contrast, use of a bis(π-allyl)Ni precursor leads to a catalyst which is about 2−4 times less active (entries 8−10). As we discussed elsewhere, the principle (π-allyl)$NiPN_2$ product formed from this precursor and the phosphorane is *inactive* in ethylene polymerization.[11] We concluded that catalyst formation involved competing reductive elimination of the Ni(II) π-allyl complex to form Ni(0)−diene or ethylene complexes in the presence of ethylene (eq 2). These would be expected to react in the same manner with phosphorane **1** as $Ni(COD)_2$ or $Ni(C_2H_4)_3$ to form an active catalyst.[9]

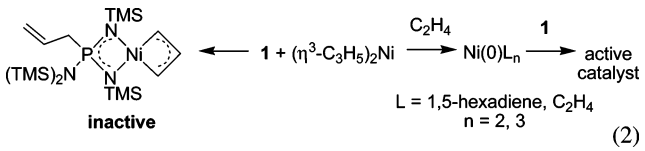

(2)

So the lower activity observed using bis(π-allyl)Ni likely reflects diminished production of these Ni(0)-alkene or diene complexes.[14] In agreement with this finding, the more thermally stable bis(π-methallyl) complex, which is less prone to reductive elimination than the parent compound,[15] gave rise to the least active catalyst (entry 10).

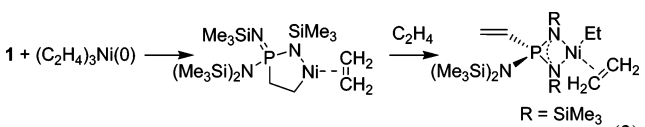

(3)

Earlier work from the Fink group had demonstrated that the principle product formed from $Ni(C_2H_4)_3$ and phosphorane **1**

Table 1. Ethylene Polymerization Using Phosphorane 1 and Ni(COD)$_2$ or Bis(π-allyl)Ni Complexes[a]

entry	[Ni]	C_2H_4 (psig)	[1-hexene] (M)	t (h)	A[b]	M_w ($\times 10^3$)	PDI
1	Ni(COD)$_2$	300	0.94	0.30	51.0	12.3	2.2
2	Ni(COD)$_2$	300	0.94	3.0	26.0	25.6	2.2
3	Ni(COD)$_2$	30	0.94	0.30	20.0	2.9	2.3
4[c]	Ni(COD)$_2$	30	0.94	0.33	12.5		
5	Ni(COD)$_2$	30	0.23	1.9	5.90	4.6	1.6
6[d]	Ni(COD)$_2$	30	0.23	4.0	2.50	11.8	2.2
7	Ni(COD)$_2$	30	0.0	4.0	1.50	61.2	2.7
8	Ni(η^3-C_3H_5)$_2$	15[e]	0.0	12.0	0.40	215[f]	1.8
9	Ni(η^3-C_3H_5)$_2$	450	0.0	4.0	0.79	109	2.2
10	Ni(η^3-2-MeC_3H_4)$_2$	450	0.0	14.0	0.034	158	2.2

[a] Toluene with [Ni] = 4.0 mM at 25 °C unless otherwise noted. In each case the Ni complex was added to the phosphorane and ethylene via syringe or over-pressurized sampling vessel. [b] Activity in kg of PE/mol of Ni × h. [c] Polymerization T is 60 °C. [d] Polymerization in the presence of 4-Me−1-pentene. [e] Initial addition of π-allyl at 15 psig followed by pressurization to 450 psig. [f] Bimodal MWD—only the MW of the major high MW component is reported.

was the *stable* ethylene, 1-nickela-2-aza-3-phospholidine complex shown in eq 3.[9c] This was thought to rearrange to a NiPN$_2$ complex in situ in the presence of ethylene inferring that the PN$_2$ complex was the active catalyst.

We thus prepared the PN$_2$NiPh(PPh$_3$) complex **2** by the route shown in eq 4. Complex **2** was obtained in 48% yield and was characterized by X-ray crystallography. Unfortunately, the structure features a disordered N(SiMe$_3$)$_2$ group and this disorder could not be accurately modeled (see Supporting Information). Nevertheless, the structure is similar to that reported for [Ph$_2$P(NSiMe$_3$)$_2$Ni(PPh$_3$)Ph].[11]

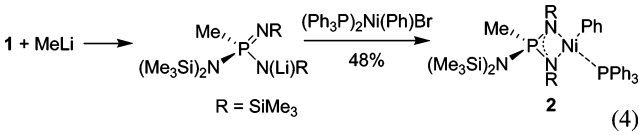

(4)

Complex **2** was evaluated for ethylene polymerization at 290 psi and 25 °C. Unlike its less hindered analogue, complex **2** produces branched ethylene oligomers in the *absence* of a PPh$_3$ scavenger but at very low activity (2 g PE/mol Ni × h). In the presence of a 10-fold excess Ni(COD)$_2$ the activity improves somewhat (42.5 g PE/mol Ni × h). The low activity of these systems is a consequence of *reversible* and unfavorable scavenging of PPh$_3$, coupled with the low equilibrium solubility of ethylene (ca. 0.2 M) under these conditions.[11] In essence, the resting state during catalysis is a PN$_2$Ni−R(PPh$_3$) complex, in which PPh$_3$ can be *reversibly* sequestered by, e.g., Ni(COD)$_2$ but ethylene must displace PPh$_3$ prior to *each* insertion (eq 5).

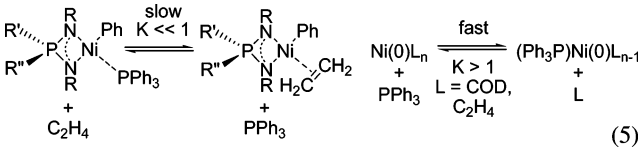

(5)

The branched material formed under these conditions was analyzed by ^{1}H and ^{13}C NMR spectroscopy and is similar in structure to the PE formed using the Keim catalyst formulations (vide infra, see Supporting Information). We also note that ethylene polymerization by the Keim catalyst formulations is completely inhibited by the addition of 1 equiv of PPh$_3$. We thus conclude that the active species is a sterically hindered NiPN$_2$ complex as hypothesized by Fink and co-workers.

The polymers formed using the Keim catalysts vary from low MW oligomers to high MW polymer depending on conditions and usually have a narrow MWD with $M_w/M_n \sim 2$. In the presence of large quantities of α-olefins only low MW materials are produced, although for longer polymerization times and smaller amounts of α-olefin, resins with a bimodal MWD were occasionally formed, presumably due to depletion of the added α-olefin which functions as a chain transfer agent. The MW of the polymer formed is also sensitive to ethylene pressure; this was revealed by an experiment where the catalyst was generated at 15 psig ethylene followed by subsequent pressurization to 450 psig (entry 8). The polymer formed had a bimodal MWD with a small quantity of low MW material being formed (Figure 2). Also, by comparison of entries 1−3, it can be seen that the MW of the material formed is higher at higher P in the presence of 1-Hx.

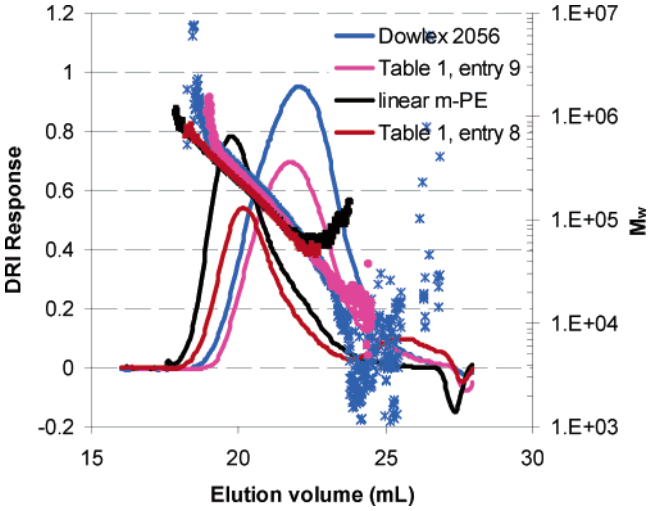

Figure 2. Plot of refractive index detector (DRI) response (arbitrary units) vs elution volume for Dowlex 2056, a metallocene PE sample and PE samples prepared using the Keim catalyst. The light-scattering signal for each sample is depicted in the form of log(M_w) vs elution volume.

It is known from the work of Yano and co-workers that only small quantities of α-olefins are needed for enhanced activity [presumably through in situ formation of more reactive Ni(0)−alkene complexes], and under these conditions, higher MW polymers can be produced.[10] We deliberately chose rather high levels of α-olefin with a view to studying their incorporation into the polymer (vide infra).

The higher MW polymer samples (entries 7−10) were analyzed by GPC at elevated temperature using a three-angle, light scattering detector.[16] Samples of Dowlex 2056, a broad MWD LLDPE sample, and a HDPE sample prepared using Cp*$_2$ZrCl$_2$/PMAO (prepared at 70 °C, 75 psig C_2H_4 in toluene using 1000:1 Al:Zr, M_w = 232 kg/mol, PDI = 1.5) were used as standards for the purposes of a branching analysis. Because

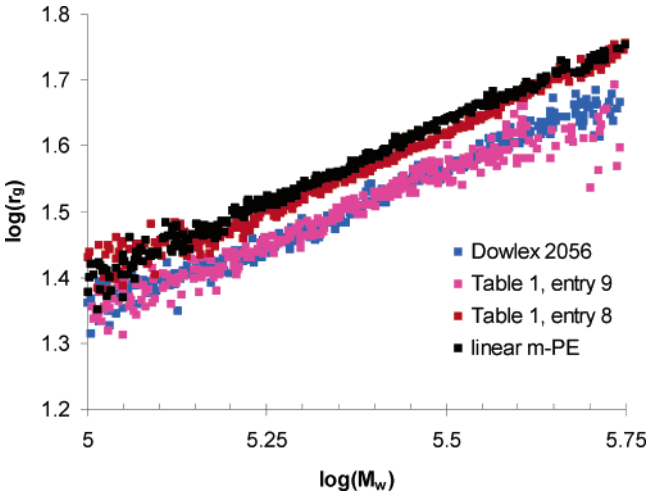

Figure 3. Log radius of gyration (r_g) vs log(M_w) for two PE samples prepared using phosphorane **1** and Ni(η^3-C_3H_5)$_2$, Dowlex 2056 and a metallocene-catalyzed linear PE. Only the linear, noise-free portion of these curves are depicted.

of the narrow MWD of the synthetic samples and lower average MW of the Dowlex PE standard, only partial coincidence of the MW distributions was achieved as the traces in Figure 2 illustrate. In particular, the Dowlex PE standard has a similar MWD to that of the PE prepared at 450 psig (Table 1, entry 9) while that of the metallocene-catalyzed PE is similar to the higher MW component of the sample prepared between 15 and 450 psig (Table 1, entry 8).

These standards and the unknowns do not have the same average composition, a requirement for an accurate branching analysis.[16] This is illustrated in Figure 3 where log(r_g) vs log(M_w) is plotted for the different samples analyzed. The samples prepared using the Ni catalysts show slightly depressed values of r_g vs M_W compared with the "linear" standards of the same MWD. However, it is not obvious that the slopes of these curves differ significantly from one another as would be expected from a linear vs (randomly) branched material. Part of the problem is that the synthetic samples lack significant quantities of high enough MW material where the deviation from linear behavior would be most pronounced.

As illustrated in Figure 4a, using the metallocene-catalyzed HDPE as the linear standard and assuming trifunctional branching with these polydisperse samples, the LCB per macromolecule was calculated using the Zimm−Stockmayer formalism.[16] For the branched PE sample with a similar MWD to the standard (red curve), a roughly constant branching frequency of 0.3 LCB per macromolecule is indicated over the MW range where the light scattering data can be considered reliable.

On the other hand the lower MW Ni-catalyzed PE sample (and even the Dowlex standard!) exhibit anomalously high branching frequencies. Since the average composition of the two PE samples prepared using the Keim catalyst are almost indistinguishable (vide infra), we are forced to conclude that this result is spurious and reflects poor overlap of the MWD (Figure 2). In agreement with this assessment, comparison of the lower MW PE sample prepared using the Keim catalyst with Dowlex 2056 gave more reasonable results (Figure 4b). It can be concluded that these samples do possess sparse levels of LCB[17] where the amounts are comparable to those seen for a Dow Insite copolymer.[2]

Most of the samples prepared were analyzed by ^{13}C NMR spectroscopy at 187.5 MHz and a typical spectrum appears in Figure 5. In addition to Me and Hx$^+$ branching, low levels of Et, ^{n}Pr, ^{n}Bu, and ^{s}Bu branches could be detected. *n*-Pentyl (*n*-Pn) branches were at the detection limit at the concentrations and acquisition times employed and unfortunately overlapped with signals due to $-CH_2CH{=}CHCH_2-$ end groups that were identified in low MW samples through gHSQC spectra.

Summarized in Table 2 are the branching distributions as estimated from integration of these quantitative ^{13}C NMR spectra. On the basis of averaged data (Table 2, entries 6−7), both total branching as well as the nature/amount of the branches present was rather insensitive to changes in either ethylene pressure (*P*) or the presence of α-olefin under the conditions investigated. The only significant difference noted involves the use of Ni(COD)$_2$ vs Ni(π-C_3H_6)$_2$ as catalyst precursor. In the latter case, Hx+ branching was reduced from that seen using the Ni(0) precursor (Table 2, entry 8)—of course the structure of the catalyst formed in situ is likely to differ with respect to substitution on P in that case.[8−11]

The samples corresponding to entries 1 and 2 were prepared and analyzed under similar conditions. It may be tentatively concluded that total branching, as well as the intensity of some of the longer branches, and ^{s}Bu branching, in particular, is marginally higher at low vs high P. While these findings are consistent with a chain-walking mechanism, the differences are modest given the error of these measurements and suggest that chain-walking is much faster than insertion.

If one compares ^{n}Bu branching for samples 1−2 and 4, which were prepared in the presence of 1-Hx, to sample 3, it can be seen that, e.g., ^{n}Bu branching is marginally higher for these three samples as would be expected for 1,2-enchainment of 1-hexene. Moreover, the highest levels are seen for material prepared with larger quantities of 1-Hx present and at lower P (i.e., entries 1 vs 2 vs 4) in accord with a copolymerization mechanism. However, the absolute increase in ^{n}Bu branching is miniscule and corresponds to ≤0.10 mol % (0.31 wt %) incorporation at the highest concentration of 1-Hx investigated. Given the low MW of many of these samples (Table 1) it is quite possible that 1-Hx is incorporated only at the chain-ends, following either 1,2- or 2,1-insertion and β-H elimination, or alternately β-H transfer to 1-Hx.

The 750 MHz ^{1}H NMR spectra of these low MW materials in *p*-DCB-d_4 revealed signals due to vinyl or internal vinylene end groups with the latter predominating; vinylidene groups were absent. This would suggest that if 1-Hx is incorporated at the chain ends, insertion would have to occur with 2,1-regioselectivity. This is not what is seen in homopolymerization of α-olefins with this same catalyst where 1,2-insertion (followed by chain-walking) dominates at low *T*.[9]

On the other hand, 1-Hx could function as a chain transfer agent involving direct β-H transfer to this coordinated alkene (or indirect via insertion into Ni−H). Depending on the regioselectivity of this process, one could form a Ni−^{n}Hx or Ni−^{s}Hx end group. The former would be indistinguishable from a "normal" chain end while the latter should give rise to signals characteristic of Me and ^{n}Bu branching where the signals due to 3B$_4$, 4B$_4$, and, to a much lesser extent, 2B$_4$ would be perturbed from their normal positions. There are numerous weak and unassigned signals present in these samples, including one that is close to 2B$_4$ (Figure 5), which might arise from such end groups. Unfortunately, these signals are also found in the polymers prepared in the absence of 1-Hx, so a definitive study will require the use of ^{13}C-labeled material to determine the fate of the added α-olefin.

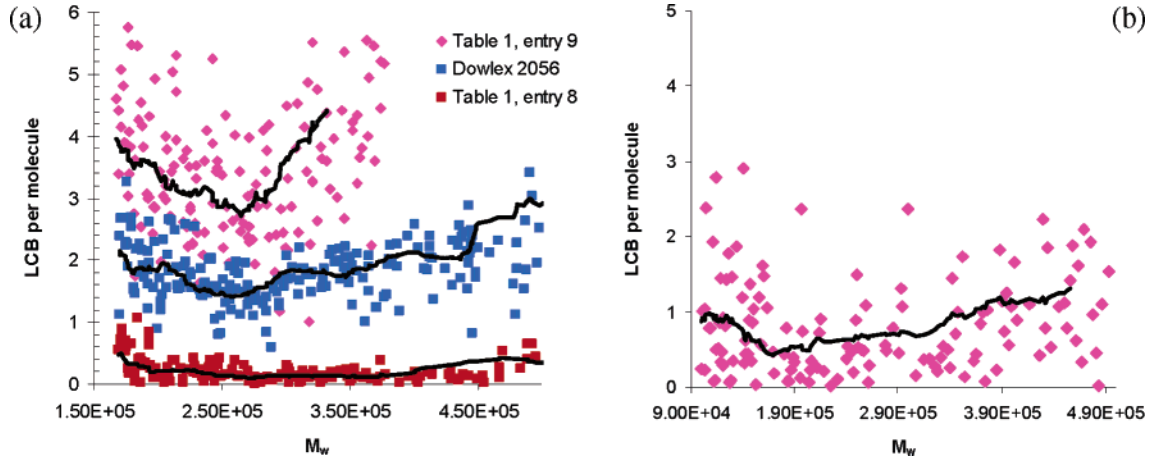

Figure 4. (a) Long chain branching (branches per molecule) vs M_w using a metallocene-catalyzed PE as a linear standard. (b) Long chain branching vs M_w for the branched PE sample (Table 1, entry 9) using Dowlex 2056 as the linear standard. Solid lines are a moving average fit to the raw data as a guide for the eye.

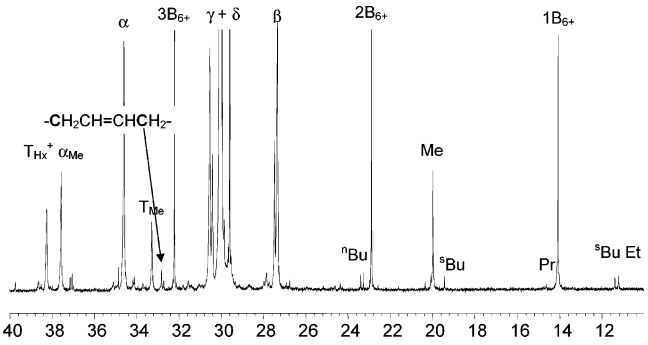

Figure 5. ^{13}C NMR spectrum of branched PE (187.5 MHz, 10 wt % in *o*-DCB-d_4:TCB 60:40, 120 °C, 2048 transients).

Similarly, when using 4-MP, weak Me groups were detected in the copolymer using an gHSQC pulse sequence. In particular, correlation of CH_3 protons at δ 0.89 with a ^{13}C signal at δ 22.89 is seen as shown in Figure 6. The position of this signal is the same as that reported in the literature for the ^{i}Pr methyl groups in poly(ethylene-*ran*-4-MP).[18] At somewhat higher field (δ 22.71) a more intense correlation is seen with a signal at δ 0.87—the order and difference in ^{13}C shift between these two signals is in agreement with that for an ^{i}Pr group at the end of a long chain.[18b] However, these groups could arise through 2,1- and 1,2- insertion, respectively, of 4-MP into Ni−H rather than through copolymerization. There are additional correlations seen at δ 23.25 and a weaker signal at δ 23.51 which are also due to CH_3 groups. These could be due to ^{i}Pr end groups with unsaturation at the γ-position (i.e., *cis*- and *trans*-^{i}Pr−CH_2CH═CHCH$_2$−Pn), given the smaller Grant and Paul parameters for a C═C vs a C−C bond, although this assignment must be viewed as tentative.

It can be concluded that copolymerization of α-olefin is not competitive with ethylene insertion in these materials and that the main function of α-olefin is to act as a chain transfer agent where much if not all of the material is incorporated at the chain ends. If so, it is unclear how LCB arises in these materials. The levels indicated by light scattering (≤1 LCB/1000 C atoms) are a significant percentage of total longer branches present by NMR (13−19 Hx^+/1000 C atoms). If macromonomer incorporation through copolymerization was involved in this process[3] it would have to be a great deal more efficient than incorporation of either 1-Hx or 4-MP. It is unclear how this could be possible given both the lower concentration of C═C bonds in a macromonomer as well as the (predominant) internal nature of this unsaturation.

With a view to clarifying this issue, DFT studies of the insertion, chain transfer and chain-walking processes were undertaken using combined QM/MM techniques and a reasonable model for the active catalyst involved in these polymerizations (Figure 7). These computational studies will be discussed in more detail elsewhere,[19] but their findings are summarized here to facilitate discussion.

The active catalyst is a sterically hindered $PN_2NiR(L)$ complex where barriers for ethylene insertion are between 17 and 20 kcal mol^{-1} and ethylene complexation energies are modest (10−12 kcal mol^{-1}), and while the barriers to chain-walking are low (7−10 kcal mol^{-1}), they are dependent on the structure of Ni−R.

Interestingly enough, there are two lower energy transition states for insertion into a 1° Ni−R or a 2° Ni−CH(Me)R that differ in the orientation of the Ni−R group in the puckered, 4-membered ring (Figure 7). Counter-intuitively, the structures with a pseudoaxial R group are lower in energy than those with a pseudo-equatorial R group by 2−3 kcal mol^{-1}. Space-filling models reveal that, for R groups larger than Me, a repulsive interaction is present between an in-plane $NSiMe_3$ group on the ligand and the R group when it is pseudo-equatorial and that this is only partially relieved in the optimized transition structure at the expense of distorting the four-membered ring (Figure 8). Of course for higher 2° Ni−R, one has to place a larger group pseudo-equatorial and so the insertion barriers are higher; calculations on Ni−2- vs Ni−3-pentyl are also consistent with this finding.

The short chain branching distribution can be understood with reference to the processes depicted in Scheme 1 where the energies etc. are based on the DFT calculations on isomeric Ni−Bu complexes. Initial chain-walking from a 1° Ni−R to a α-Me-branched Ni−R is more facile than subsequent chain-walking steps. If the latter species is generated, it has a high tendency to be trapped via insertion or "walk-back" in a degenerate fashion compared to further chain-walking. Since the chain-walking process has a higher barrier than insertion into the higher alkyls (relative to the common π-complex) it is clear why Me branching dominates over Et, ^{n}Pr, ^{n}Bu, etc.

However, is it less clear how LCB could arise based on the energetics depicted in Scheme 1. In particular, insertion is predicted to be more favorable than chain-walking for higher secondary Ni−alkyls. Using the enthalpy differences for the

Table 2. Branching Distributions for PE Samples (Branches/1000 C Atoms) Prepared Using Phosphorane 1 and Ni(COD)$_2$ or Ni(π-C$_3$H$_6$)$_2$ under Different Conditions

entry	1	2	3	4	5	6	7	8
	[1-Hx]	[1-Hx]	[1-Hx]	[1-Hx]	[4-MP]	average		table 1
conditions	0.94 M	0.94 M	0.00 M	0.23 M	0.23 M	(entries 3−5)	σ	entry 9
$P_{C_2H_4}$ (psig)	300	30	30	30	30	30		450
Me	12.16	15.90	13.95	13.16	12.04	13.05	0.96	12.8[a]
Et	0.56	0.64	0.40	0.57	0.60	0.52	0.11	--
^{n}Pr	0.30	0.69	0.55	0.57	0.42	0.51	0.08	--
^{n}Bu	0.55	0.86	0.33	0.56	0.25	0.38	0.16	--
^{n}Pn	0.21	0.18	0.13	0.14	0.11	0.13	0.02	--
Hx$^+$	19.22	17.72	13.59	16.33	15.24	15.05	1.38	8.2[a]
^{s}Bu	0.56	0.80	0.34	0.71	0.62	0.56	0.19	--
total	33.56	36.78	29.31	32.04	29.29	30.21	1.59	21.0

The data were obtained from a sample analyzed at 100 MHz. Because of solubility and sensitivity limitations, only the most intense branches were detected.

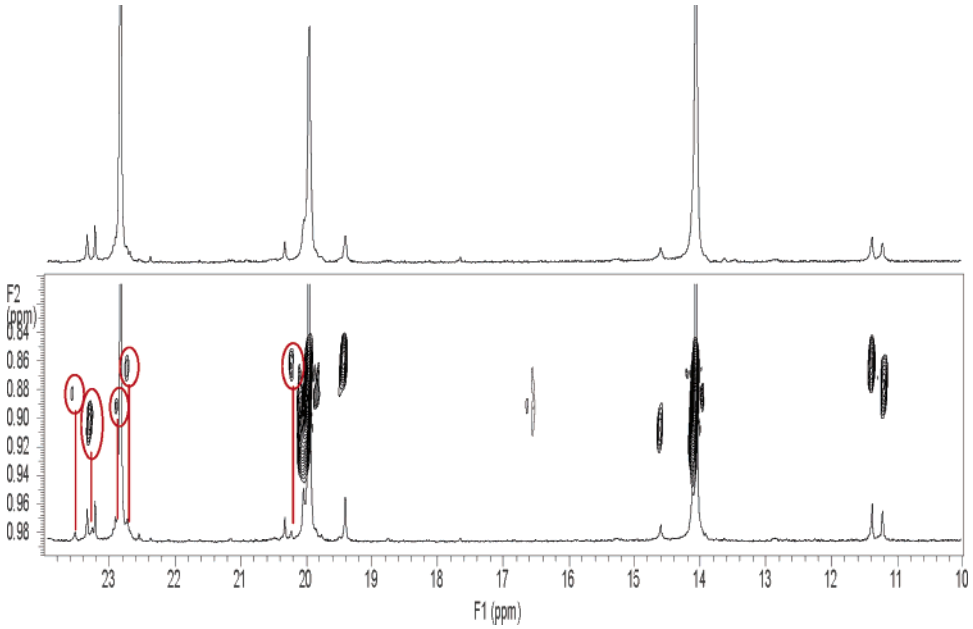

Figure 6. gHSQC ^{1}H−^{13}C NMR spectrum and ^{13}C NMR spectra of PE prepared in the presence (bottom) vs absence of 4-MP (top). Signals due to ^{i}Pr groups are highlighted in red.

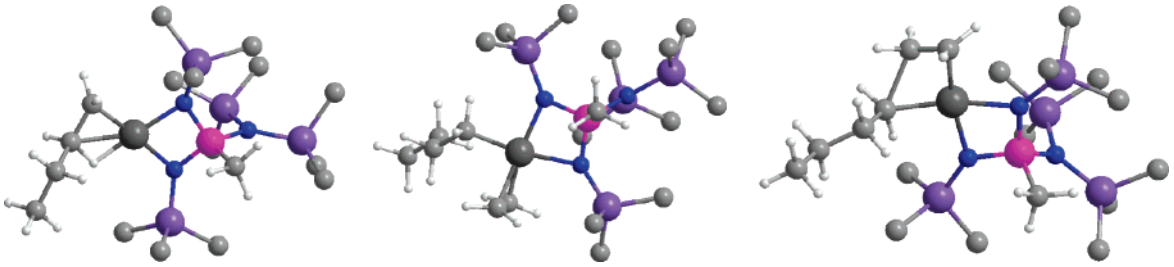

Figure 7. Chem-3D depiction (most H atoms omitted) of DFT QM/MM-optimized structures of a model for the Keim catalyst [(Me$_3$Si)$_2$NP(Me)-(NSiMe$_3$)$_2$Ni−^{n}Bu]: (a) agostic alkyl, total energy = −6.201601 au (+free C_2H_4 = −7.356368 au); (b) π complex, total energy = −7.375804 au (ΔE = −12.20 kcal mol^{-1}); (c) insertion transition state (C−C 2.057 Å), total energy = −7.347606 au (ΔE = +5.5 kcal mol^{-1}).

various species depicted in Scheme 1, stochastic simulation of chain growth[13] was undertaken using a modified algorithim that allowed for differences in the barriers for chain-walking, as well as insertion, as a function of metal position along the chain. The algorithm is similar to that developed in connection with copolymerization of ethylene and propene using models for Ziegler−Natta catalysts.[20]

The integrity of such a simulation relies first and foremost on the quality of the generator of uniform deviates. We believe that the generator based on the example ran2[21] performs sufficiently well for this purpose. The model was based on transition state theory and utilized the ratio of chain-walking to insertion probabilities defined in eq 6.

$$\frac{\pi_{cw}}{\pi_{ins}} = \frac{R_{cw}}{R_{ins}} = \frac{k_{cw}[\beta_o]}{k_{ins}[\pi_o]} = \frac{k_{cw}}{k_{ins}K_{eq} \times P} \qquad (6)$$

where k_{cw} and k_{ins} denote the respective rate constants for chain-walking and insertion, K_{eq} is the equilibrium constant of ethylene complexation, and P is the monomer pressure. The assumptions here are that the ratio of microscopic reaction probabilities π_{cw}/π_{ins} is equal to the ratio of macroscopic reaction rates (R_{cw}/

Scheme 1. Chain-Walking vs Insertion Barriers and Probabilities of Insertion vs Chain-Walking for Isomeric Ni−Bu Complexes

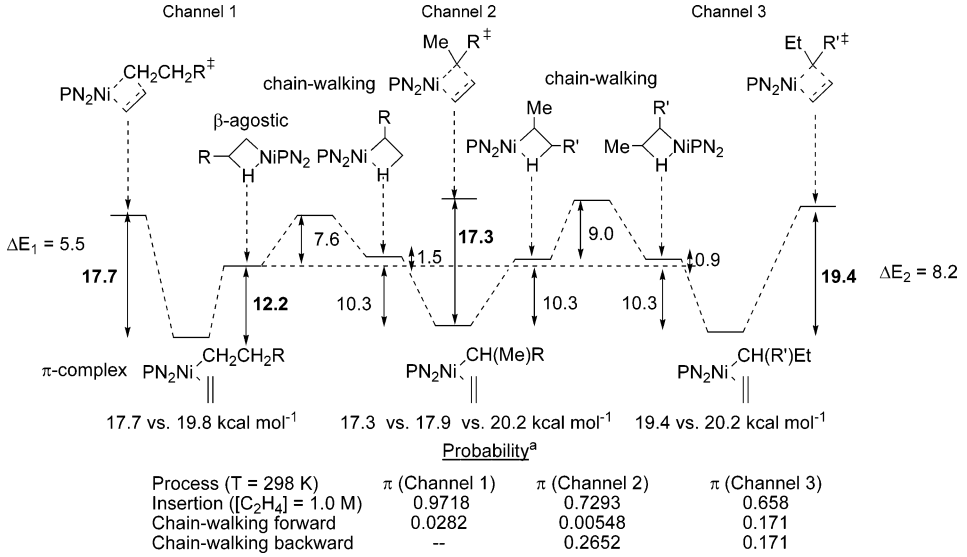

Probability[a]

Process (T = 298 K)	π (Channel 1)	π (Channel 2)	π (Channel 3)
Insertion ([C_2H_4] = 1.0 M)	0.9718	0.7293	0.658
Chain-walking forward	0.0282	0.00548	0.171
Chain-walking backward	--	0.2652	0.171

[a] Probabilities (π) are calculated with respect to a given agostic alkyl β using eq 6 without inclusion of entropy changes on ethylene binding or normalization.

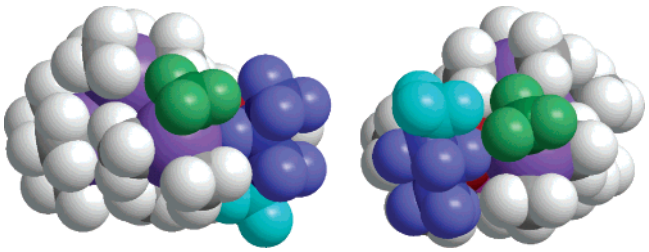

Figure 8. Space filling models of the transition structures for insertion of C_2H_4 into Ni−^{s}Bu with a pseudoaxial vs pseudo-equatorial Et group. The ^{s}Bu group is highlighted in blue, while the Me group of the ethyl moiety is highlighted in cyan and a Me group on a $SiMe_3$ group is highlighted in green.

R_{ins}) and that a given metal alkyl (β_o) is in thermodynamic equilibrium with its corresponding π complex (π_o) through binding of ethylene (i.e., $K_{eq} = [\pi_o]/[\beta_o] \times P$). It was also assumed that the entropy change on ethylene binding corresponded to $T\Delta S_o = -8.9$ kcal mol^{-1} at 298 K in determining the value of $K_{eq} = \exp[-(\Delta H_o - T\Delta S_o)/RT]$ which was assumed constant regardless of Ni−R.[13]

The simulation can take place in one of the three channels (Scheme 1): primary alkyls (1), secondary NiCH(Me)R alkyls (2), and higher secondary alkyls (3), with possible multiple crossings between them. The simulation starts from the polymer chain represented by the *n*-butyl group (channel 1) and proceeds via two possible events: (1) insertion or (2) chain-walking to a secondary alkyl, which is chosen by means of a random number, and which is generated based on the probability defined by eq 6. If the chain-walking event is selected, the process switches to channel 2, where there are three possible events: insertion, chain-walking back to channel 1 or chain-walking forward to channel 3. Since the rates of insertion and chain-walking reactions are different for each channel, the probabilities are recalculated each time the simulation crosses to a different channel.

The whole process is repeated until $X_n = 4000$ was attained during this simulation. This value was selected based on the highest MW polymer formed (Table 1). The output is a one-dimensional matrix, whose elements represent the length of the branches at each of the C atoms along the (main) polymer chain: 1 if there is no branch, 2 if there is a methyl branch, etc. The results of the simulation for $T = 298$ K are given in Table 3 and were statistically validated through 1000 repetitions using two different models.

One (model I) is based on the energetics depicted in Scheme 1, and another where insertion into *all* 2° Ni−R involved a barrier of 19.5 vs 18.0 kcal mol^{-1} for insertion into 1° Ni−R (model II) so as to illustrate the differences etc. As shown in Table 3, the use of Model I led to more intense Me branching under all conditions vs model II where the SCB distribution is more evenly distributed. Although the experimental SCB distribution is not exactly reproduced using the DFT energetics, it is clear that a lower insertion barrier into Ni−α-Me−R vs all other 2° Ni−R is responsible for the observed distribution. Further, the total levels of branching are apparently governed by the difference in energy between insertions into 1° vs 2° Ni−R.

What the simulations fail to reproduce is the weak *P* dependence observed for branching with this catalyst. It is possible that our estimate for the entropy change on ethylene binding is inaccurate and thus the value of K_{eq} in eq 6 is inappropriate or differs depending on the nature of Ni−R. Also, our assumption that the alkyls are *only* in equilibrium with their corresponding π complexes is probably invalid, particularly when the chain-walking barriers (7−10 kcal mol^{-1}) are equivalent in energy to the ethylene uptake barrier (largely entropic in nature and ca. 9 kcal mol^{-1} at 298 K[22]).

What is not even qualitatively reproduced by these simulations is the observed intensity of the Hx^+ branching. Earlier simulation work indicates that LCB formation is only possible when there is a large difference in 1° vs 2° insertion rates (i.e., >5 kcal mol^{-1} difference in barriers) and chain-walking is fast compared to 2° insertion.[13] The DFT calculations do not support such a large energy difference at least for the structures examined to date.

To further address this issue, we also performed some modeling of the experimental branching distributions using a simplified, analytical model developed earlier to describe branching in PE prepared with Ni α-diimine catalysts.[12] The assumptions in this model are that branches are isolated by at least 2 C atoms (which is reasonable since consecutive branches were not detected in these materials) and that the metal cannot walk past a branch point.

Table 3. Number of Branches Per 1000 C Atoms at Various *T*, *P*, and Probabilities of Events at $T = 298$ K

Branching at 298 K									Me branching vs. T, P (Model II)				
P (psi)	15	30	300	450	15	30	300	450	T(K)	15	30	300	450
Branch	Model I				Model II				278	4.76	3.87	3.00	2.94
Me	35.50	32.78	14.44	11.12	7.05	5.53	4.19	4.10	298	7.05	5.53	4.19	4.10
Et	0.55	0.29	0.03	0.02	2.11	1.29	0.35	0.27	318	9.92	7.73	5.56	5.42
^{n}Pr	0.29	0.16	0.01	0.00	1.07	0.61	0.09	0.05	338	9.86	7.74	5.59	5.44
^{n}Bu	0.13	0.07	0.00	0.00	0.52	0.26	0.02	0.01	Chain-walking vs. insertion at 298 K (Model II)[a]				
^{n}Pn	0.07	0.04	0.00	0.00	0.26	0.14	0.00	0.00	π_{ins}	0.121	0.216	0.738	0.811
^{n}Hx	0.04	0.01	0.00	0.00	0.13	0.06	0.00	0.00	π^{f}_{cw}	0.442	0.395	0.134	0.098
Total	36.58	33.35	14.48	11.14	11.14	7.89	4.65	4.43	π^{b}_{cw}	0.437	0.389	0.128	0.091

[a] π_{ins} is the (averaged) probability of insertion, while π^{f}_{cw} and π^{b}_{cw} are the (averaged) probabilities of walking forward and backward from a given metal alkyl.

Table 4. Experimental vs Theoretical Mole Fractions of Branches of Various Length[a]

	1-Hx (0.94 M)						1-Hx (0.23 M)		4-MP (0.23 M)	
	entry 1 (300 psig)		entry 2 (30 psig)		entry 3 (30 psig)		entry 4 (30 psig)		entry 5 (30 psig)	
Me	0.379_1	0.379_8	0.453_9	0.453_6	0.487_8	0.487_6	0.433_0	0.433_1	0.432_3	0.432_4
Et	0.016_6	0.012_3	0.017_5	0.017_2	0.013_8	0.012_5	0.017_7	0.015_0	0.020_5	0.012_2
Pr	0.009_0	0.012_1	0.018_7	0.016_7	0.018_6	0.012_4	0.017_7	0.014_7	0.014_3	0.012_1
Bu	0.016_4	0.011_8	0.023_5	0.016_1	0.011_4	0.011_9	0.017_5	0.014_2	0.008_6	0.011_7
pnt	0.006_2	0.011_6	0.004_8	0.015_7	0.004_6	0.011_8	0.004_4	0.013_9	0.003_8	0.011_6
Hx^+	0.572_7	0.572_5	0.481_6	0.480_7	0.463_9	0.463_7	0.509_6	0.509_2	0.520_5	0.520_0
Model Parameters[b]										
K	0.984		0.976		0.996		0.979		0.992	
λ	0.993		0.985		0.960		0.988		0.974	
θ	0.033		0.039		0.027		0.036		0.029	
RSS[c] ($\times 10^4$)	0.787		1.79		0.929		1.18		1.44	

[a] Experiments correspond to those listed in Table 2. For each entry, the first column is the experimental data while the second contains theoretical estimates. [b] For definition of these parameters, see the text. [c] Residual sum of squares.

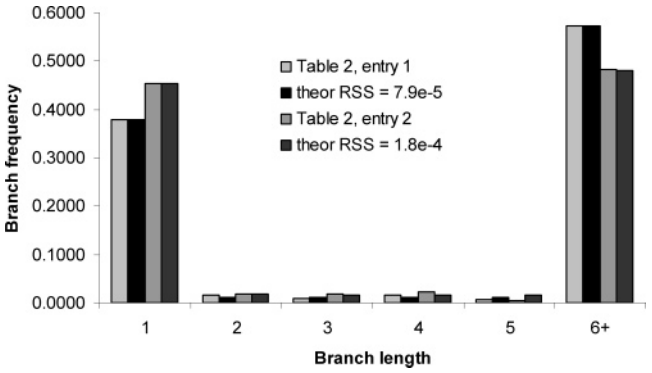

Figure 9. Experimental vs theoretical mole fraction of branches as estimated using an analytical model based on the kinetics of chain-walking vs insertion.[12]

This latter assumption is not valid here but the low levels of ^{s}Bu branching observed under all conditions (<1 C/1000 C atoms) suggest that this simplified model will prove adequate. For the purposes of modeling, the intensity of the latter signal was included with that due to Me branching since formation of a Me branch must precede formation of a ^{s}Bu branch. Finally, it was assumed that, for the purposes of modeling, only the kinetic constants associated with a 1° NiR and 2°-NiCH(Me)-R′ were unique, which is the simplest version of this model that is consistent with the DFT calculations.

If the intensity data for branches of all lengths are used, the fit of the model to the data is good, at least for Me and Hx^+ branching (Figure 9), but the basic parameters that emerge (Table 4) are troubling. These parameters are defined in ref 12a but are provided here in simplified form:

$$K = \frac{k_w/\phi}{1 - (k_w/\phi)K} \quad \text{and} \quad k_w/\phi = \frac{k_w}{2k_w + k_p[M]} \tag{7}$$

where k_w/ϕ is the probability of chain-walking in either direction for 2° alkyls other than Ni−CH(Me)R′.

$$\lambda = \frac{1 - \pi_1}{1 - \sigma\pi_1} \quad \text{and} \quad \pi_1 = \frac{k_f^1}{k_f^1 + k_p^1[M]} \tag{8}$$

where π_1 is the probability of chain-walking from a 1° to a 2° alkyl, k_f^1 and k_p^1 are the rate constants for chain-walking vs propagation with

$$\sigma = \frac{k_b^2 K_2}{k_f^1} = \frac{k_b^2}{k_b^2 + k_p^2[M] + k_w(1 - K)} \tag{9}$$

where k_b^2 and k_p^2 are the rate constants for walking backward vs trapping and insertion into Ni−CH(Me)R′, and $\theta = k_p/k_p^2$ is the ratio of propagation rate constants for insertion into higher 2° alkyls vs Ni−CH(Me)R′.

A brief perusal of the results obtained indicate that $K = \lambda \sim 1$ while θ varies somewhat for the different experiments and is much less than one. However, if the same catalyst is generated

under the different conditions, and this certainly must be true of experiments conducted in the presence of 1-Hx, θ should not vary at all. In any event, the average value obtained $\theta = 0.0328$ is in very good agreement with that estimated from the DFT results (0.0290).

A value of $\lambda \sim 1$ means that $\sigma \sim 1$ (eqs 8 and 9) and that $k_b^2 >> k_p^2[M] + k_w(1 - K) \Rightarrow k_b^2 >> k_p^2[M]$ if $K \sim 1$ as the modeling indicates. This finding is partly consistent with the DFT results in that walking backward from Ni−CH(Me)R′ is favored over other processes, at least at sufficiently low *P* (Scheme 1, Table 3).

$K \sim 1$ implies that $k_w/\phi = 0.5$ (eq 7) or that the probability of chain-walking (in either direction) is effectively unity once the metal migrates down the polymer chain past C-2. There is no support for this finding based on the DFT results except at low P using model II (see Table 3). Thus, at present, there is a disagreement between simulations based on DFT results vs experimental behavior (and kinetic modeling thereof) which cannot be readily rationalized.

While chain-walking will become more probable compared to insertion if we have underestimated the ethylene capture energetics, one suspects this error should be more or less uniform for both 1° and 2° Ni−R. On the other hand, as suggested by Escobedo and co-workers,[23] perhaps ethylene binding and insertion exhibits a chain-length dependence, becoming increasingly unfavorable as the metal migrates down the chain. One can estimate that the change would have to correspond to an energy increase of ca. 3−4 kcal mol^{-1} at 298 K in the insertion barrier in order to account for the kinetic modeling results vs the DFT calculations. This assumption (i.e., a 366-fold decrease in ethylene binding constants or insertion rates) seems unreasonable.

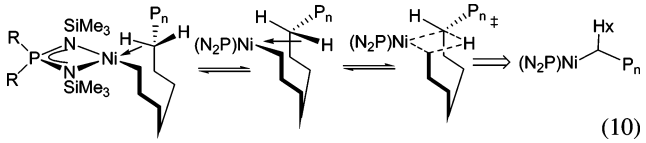

(10)

So it is still unclear what process is responsible for LCB formation in these systems. While macromonomer incorporation through copolymerization is an obvious mechanism for forming long branches,[3] the Keim catalyst is not competent for copolymerization of even simple α-olefins (vide supra). We are thus tempted to conclude that formation of Hx^+ branches in these materials may occur by a mechanism other than chain-walking.

One possibility is either intra- or intermolecular C−H activation as suggested in eq 10. Both processes have precedent in early transition metal-catalyzed olefin polymerization[24] but to our knowledge have not been documented for late metal polymerization catalysts.

The intermolecular process,[24a] in particular, provides an attractive mechanism for LCB formation in these materials that is analogous to chain transfer to polymer involved in the synthesis of LDPE. It is not clear why the formation of branches at least 6 C atoms long (eq 10) would be favored over other intramolecular C−H activation reactions[25] and the exploration of this hypothesis will be the subject of future research.

Conclusions

The poly(ethylene) formed using the Keim catalyst in fact *closely* resembles low-density PE both with respect to the nature of the short and long chain branching present in these materials. Unfortunately, over the narrow *T* and *P* ranges studied, the short chain branching is rather insensitive to changes in experimental conditions although this limitation is more a function of catalyst instability and thus activity. Although α-olefins enhance the activity of the Keim catalyst, they are only incorporated at the chain-ends following, or prior to, chain transfer. DFT calculations coupled with stochastic simulation of chain growth are in reasonable agreement with the short chain branching distribution as determined by ^{13}C NMR spectroscopy given the assumptions involved in the simulation process. Kinetic modeling of polymer microstructure gives results that are inconsistent with the DFT calculations if Hx^+ branching is included as arising from chain-walking. These results could point to a new mechanism for the formation of longer branches in these materials.

Experimental Section

All materials were obtained from Aldrich or Strem, and purified as required, unless otherwise noted. All synthetic procedures were conducted under a N_2 atmosphere using Schlenk techniques or in a glovebox. Tetrahydrofuran, diethyl ether, toluene, hexane, and dichloromethane were purified by passage through activated La Roche A-2 alumina and Engelhard CU-0226s Q-5 columns.[26]

Routine ^1H, ^{13}C, and ^{31}P NMR spectra were recorded on a Varian Mercury or Gemini 300 MHz instruments. Benzene-d_6, and toluene-d_8 were distilled from Na or Na/K alloy prior to use. Methylene chloride-d_2, and chloroform-d_1 were distilled from P_2O_5 and stored over 4 Å molecular sieves. ^1H NMR spectra were referenced with respect to residual protonated solvent, while ^{13}C NMR spectra were referenced with respect to deuterated solvent. ^{31}P NMR spectra were referenced to a phosphoric acid external standard. FT−IR spectra were obtained on a DigiLab Excalibur FTS 3000 spectrometer and were not calibrated. Elemental analyses were performed either by Oneida Research Services or Galbraith Laboratories. The compounds $(PPh_3)_2Ni(Ph)Br$,[27] $Ni(COD)_2$,[28] Me_3SiN_3,[29] $[(Me_3Si)_2N-P{=}NSiMe_3]$,[30] and $[(Me_3Si)_2N-P(=NSiMe_3)_2]$ (**1**),[30] were prepared according to literature procedures.

Polymerization Experiments. Polymerization of Ethylene with Nickel(0) Complexes and Phosphorane 1. $Ni(COD)_2$ (55 mg, 200 μmol) and 45 mL of toluene were added into a 300 mL stainless steel autoclave, equipped with a glass insert, under nitrogen in a glovebox, to make a 4 mM solution. A magnetic stir bar was added for agitation. The autoclave was sealed and removed from the glovebox. While stirring, the vessel was pressurized with 30−300 psig of ethylene at 25 °C. A solution of phosphorane **1** (73 mg, 200 μmol) in 5 mL of toluene was added via syringe (30 psig) or via an over-pressurized 25 mL sample cylinder (300 psig). The mixture was stirred under ethylene at 25 °C for various times (Table 1). After venting the autoclave, the resulting solution was evaporated in vacuo. The polymer was washed with acidic methanol and dried in a vacuum oven for 12 h.

Polymerizations in the presence of 1-hexene or 4-methyl-1-pentene were conducted in the same manner except that α-olefin was added to the reactor at the same time as the $Ni(COD)_2$. These lower MW samples were generally soluble in toluene solution and so catalyst residues could be removed prior to analysis by passage through a short column of alumina.

A representative ^{13}C NMR spectrum of these materials is presented in Figure 5 (or Figure S-1c of the Supporting Information).

Polymerization of Ethylene with Bis(π-allyl)nickel and Phosphorane 1. Into a 300 mL autoclave within a glovebox were added **1** (111 mg, 400 μmol) and 100 mL of toluene to make a 4 mM solution. A magnetic stir bar was added for agitation. The autoclave was sealed and removed from the glovebox. While stirring, the vessel was pressurized with 450 psig ethylene at 25 °C. In a 25 mL stainless steel sample vessel were placed $Ni[\eta^3\text{-}(C_3H_5)]_2$ (56 mg, 400 μmol) and 5 mL of toluene. This solution was injected, and the reactor stirred at 25 °C. The resulting solution was vented and solvent evaporated in vacuo. Polymer was washed with acidic methanol and dried in a vacuum oven for 12 h. This polymerization

reaction yielded 1.3 g of PE over 4 h. A ^{13}C NMR spectrum of this material is included as Supporting Information (Figure S-1b).

A similar procedure was used in the case of Ni[η^3-(2-Me−C_3H_4)]$_2$ except that only 0.19 g PE was isolated after 14 h.

Synthesis of [(TMS$_2$N)(Me)P(═NTMS)$_2$]NiPh(PPh$_3$) (2). A solution of MeLi (5.2 mL, 1.6 M in diethyl ether, 8.3 mmol) was added to a solution of TMS$_2$NP(═NTMS)$_2$ (3.0 g, 8.2 mmol) in diethyl ether (50 mL) at −78 °C. The mixture was allowed to warm to room temperature and stirred for another 12 h. The volatiles were removed in vacuo and a colorless solid of [Li][(TMS$_2$N)(Me)P(═NTMS)$_2$][31] was obtained and used for the next step without further purification.

[Li][(TMS$_2$N)(Me)P(═NTMS)$_2$] (1.80 g, 4.65 mmol) in 15 mL of toluene was mixed with a dispersion of (PPh$_3$)$_2$Ni(Ph)Br (3.44 g, 4.65 mmol) in 10 mL of toluene for 6 h at room temperature. The resulting deep red solution was filtered through Celite, and solvent was reduced to ca. 20 mL in vacuo. Upon layering with hexane (20 mL) and cooling to −28 °C, a solid was obtained, which was mainly PPh$_3$. After all volatiles were removed from the mother liquor and the residue was washed with hexane, a yellow solid was obtained. (1.7 g, 48%). ^1H NMR (300 MHz, benzene-d_6, 298 K): δ −0.11 (s, 18H, NSiCH_3), 0.66 (s, 18H, N(SiCH_3)$_2$), 1.99 (d, J = 12.9 Hz, 3H, P*Me*), 6.45 (s, 3H, *m*/*p*-*Ar*Ni), 6.93 (s, 2H, *o*-*Ar*Ni), 6.98 (s, 6H, *p*-P*Ph*$_3$), 7.37 (s, 3H, *o*-P*Ph*$_3$), 7.83 (s, 6H, *o*-P*Ph*$_3$); ^{31}P NMR (121.1 MHz, benzene-d_6, 298 K): δ 36.7 (s, 1P, *P*N$_2$), 32.0 (s, 1P, *P*Ph$_3$). IR (Nujol, cm^{-1}): 1562 (m), 1287 (m), 1251 (s), 1115(w), 1093 (m), 1075 (s), 1019 (w), 949 (s), 897 (m), 872 (w), 846 (s), 777 (w), 742 (w) 727 (m), 701 (m), 670 (w), 617 (w). Anal. Calcd for $C_{37}H_{59}N_3NiP_2Si_4$: C, 57.06; H, 7.64; N, 5.39. Found: C, 56.90; H, 7.25; N 4.87. Single crystals were obtained by slow evaporation of a hexane solution of this compound. Details of the structure determination are included as Supporting Information.

Polymerization of C$_2$H$_4$ with Complex 2. A 300 mL reaction vessel was charged with 100 mL of toluene and a magnetic stirbar within a glovebox. In a Teflon cup, wired to the thermocouple well, was placed complex **2** (155 mg, 200 μmol). The reactor was sealed and removed from the glovebox. While being stirred, the solution was saturated at 25 °C with 290 psig of ethylene (final [C_2H_4] = 0.2 M). Addition of the complex was performed by inverting the Teflon cup, and the mixture was allowed to react for 10 h. The vessel was vented and the solution filtered through a basic Al_2O_3 column washing with hexane. All volatiles were removed in vacuum and an oligomeric PE was obtained. Yield: 4 mg. A ^1H NMR spectrum of this material is depicted in Figure S-2c and is consistent with the presence of branching as revealed by an intense signal at δ 0.86 due to terminal Me groups and weak signals due to unsaturated end groups at δ 4.95 (PE−CH═CH_2), 5.36 (PE−C*H*═C*H*-PE), and 5.80 (PE−C*H*═CH_2).

Polymerization of C$_2$H$_4$ with Complex 2 in the Presence of Ni(COD)$_2$. Into a 300 mL reaction vessel within a glovebox were added Ni(COD)$_2$ (0.55 mg, 2 mmol) and 100 mL of toluene. A magnetic stir bar was added to aid agitation. In a internal Teflon cup was placed complex **2** (155 mg, 200 μmol). The reactor was sealed and removed from the glovebox. While being stirred, the solution was saturated at 25 °C with 290 psig of ethylene (final [C_2H_4] = 0.2 M). Addition of the complex was performed by inverting the Teflon cup, and the mixture was allowed to react for 10 h. The vessel was vented and the solution filtered through a basic Al_2O_3 column washing with hexane. All volatiles were removed in vacuum and an oligomeric PE was obtained: 85 mg.

A ^1H NMR spectrum of this material is depicted in Figure S-2b. By comparison of parts b and c of Figure S-2 with part a of Figure S-2, it can be seen that the MW of the material formed using complex **2**, either in the presence or absence of Ni(COD)$_2$, is considerably higher than that formed using Ph$_2$P(NTMS)$_2$NiPh(PPh$_3$) in the presence of Rh(I).[11]

A ^{13}C NMR spectrum of this material is included as Supporting Information (Figure S-1a). The characteristic pattern of Me and Hx+ branching is also observed for this sample.

Preparation of Polymer Samples for NMR Analysis. The samples were dissolved in a 60% 1,4-dichlorobenzene-d_4:40% 1,2,4-trichlorobenzene solvent mixture to produce ca. 10 wt % polymer solutions. The samples were heated to 120 °C and rotated at 20 rpm in a Kugelrohr oven for 2 h, and then at 100 °C for 10 h more. A trace of hexamethyldisiloxane (HMDS) was added to the original solvent mixture to serve as an internal chemical shift reference both in 1D and 2D NMR spectra (^1H δ = 0.09, ^{13}C δ = 2.03).

Quantitative ^{13}C NMR experiments were performed at 188.6 MHz using a 10 mm broadband probe ($^{15}N-^{31}P$) on a Varian UNITYplus 750 MHz spectrometer at 120 °C. The experimental parameters were set as follows: 14.2 μs 90° pulse, 30 kHz spectral width, 2048 transients, 2.1 s acquisition time, and a 25 s relaxation delay for quantitative analyses.

2D gHSQC NMR. Gradient-assisted 2D HSQC (gHSQC) spectra were collected on a Varian UNITYplus 750 MHz spectrometer with a Nalorac $^1H/^2H/^{13}C$/X 5 mm PFG probe operated at 120 °C. The 90° pulse widths for ^1H and ^{13}C were 9.1 and 16 μs, respectively. Data were acquired using the following parameters: a relaxation delay of 1 s, a delay Δ set to $1/(2 \times {}^1J_{CH})$ with ${}^1J_{CH}$ = 125 Hz, and an acquisition time of 0.15 s with simultaneous ^{13}C GARP1 decoupling. A total of 8 transients were averaged for each of 2 × 1024 increments during t_1. The evolution time was incremented to provide the equivalent of an 11 kHz spectral width in the f_1 dimension, and a 4.8 kHz spectral width was used in the f_2 dimension. The PFG pulses were 2.0 ms in duration and had amplitudes of 0.214 and 0.107 T/m for the first and second PFG pulses. The experiment times were ca. 5 h. Data were zero-filled to a 4096 × 4096 matrix and weighted with a shifted sine-bell function before Fourier transformation.

GPC—Light Scattering Analyses. A Water 150C+ instrument, equipped with internal DRI and Wyatt Technology miniDawn-HT MALLS (λ = 690.0 nm, 4.95 W) detectors, was used. Samples were prepared in injection vials by dissolving polymer in eluent (ca. 0.5−1.0 wt % in 1,2,4-TCB with 1 wt %. Irganox 1010) in a 150 °C oven for a necessary period of time required for complete dissolution (typically 6−12 h depending on MW). Agitation of the vials was necessary and was accomplished by a rotating carriage within the oven chamber. Samples (250 μL injection volume) were fractionated using a set of three PLgel 10 μm Mixed-B LS columns (300 mm × 7.5 mm) eluting with TCB at 1.0 mL/min at 135 °C.

The MWD and branching calculations were performed using Wyatt Technology's ASTRA 4.70 software using a d*n*/d*c* of 0.110 and assuming 100% mass recovery. This procedure has been found more useful than calibrating the DRI detector as recommended by Wyatt Technology [using known quantities of, e.g., poly(styrene) standards] since the actual mass of polymer injected in 250 μL of a 1.0 wt % solution is polymer and MW *dependent* due to differences in solution viscosity.

A first order M_w vs V_e fit was usually employed in the determination of MW averages to reduce error associated with "scatter" of the light-scattering data at either end of the MWD. Higher order polynomial or exponential fits are not recommended because the light-scattering signal invariably trends *upward* at long elution volumes with polydisperse poly(olefin) samples having lower MW tails. It is possible using Wyatt Technology's Corona software to correct for this behavior by extrapolation from the linear portion of the light scattering curves over the entire MWD.

Only the linear portion of the light-scattering vs V_e curves were employed in the branching calculations and only where the MWD of the sample and linear standard overlapped. No correction was applied for short-chain branching or differences in composition between sample and standard. Depending on the linear standard used (Dowlex 2056 vs a metallocene catalyzed PE), different branching indices were obtained as discussed in the text.

Density Functional Theory Calculations and Simulations. All the DFT results were obtained from calculations based on the Becke-Perdew exchange-correlation functional,[32] using the Amsterdam Density Functional (ADF) program.[33] The standard double-ζ STO basis sets with one set of polarization functions were applied for H, C, N, P, and Si atoms, while the standard triple-ζ

basis sets were employed for the Ni atom.[34] The 1s electrons of C, N, and O as well as the 1s-2p electrons of P, Si, and Ni were treated as frozen core. Auxiliary s, p, d, f, and g STO functions,[35] centered on all nuclei, were used to fit the electron density and obtain accurate Coulomb and exchange potentials in each SCF cycle.

Quantum mechanical/molecular mechanical (QM/MM) modeling of the Keim catalyst used the algorithms implemented within ADF[36] where the QM part of the complex was defined as the model complex $[(H_3Si)_2N-P(H)\{N(SiH_3)\}_2]NiR(L)$ where both the R group on Ni and $L = C_2H_4$ were treated using the full QM method, regardless of chain length. Hence, the MM part consisted of substituting Si−H and P−H link atoms by $Si-CH_3$ and $P-CH_3$, respectively. An augmented Sybyl force field[37] was utilized to describe the MM potential, which included van der Waals and torsional parameters for Si and P from the UFF potential.[38]

The geometry optimization on the entire system was carried out with coupling between QM and MM atoms. In the optimization of the MM part, the Si−C and P−C distances were constrained to be 28.0 and 26.5% longer than the optimized Si−H and P−H distances in the generic complex. These constraints were also based on the UFF bond length values.[38] Electrostatic interactions were not included in the MM potential. Full details of these calculations will be reported elsewhere.[19]

Stochastic simulations of the polymer growth and isomerization were performed using our own code and the method described in refs 13 and 20. This method uses as input data the energies/activation energies of the elementary reactions in the process and is based on the assumption that the relative probabilities of two reactive events (microscopic), π_i and π_j, are equal to their relative reaction rates (macroscopic), R_i/R_j; with the probability normalization constraint, $\Sigma\pi_i = 1$. Such an approach makes it possible to model the *T* and *P* effects. More specifically, the *T* dependence appears in the probabilities for all the events through the rate and equilibrium constants (Eyring and Arrhenius equations). The *P* affects directly the relative probabilities for unimolecular (isomerization)/bimolecular (ethylene capture + insertion) events, and indirectly it influences all the probabilities because of probability normalization. A more detailed description of the stochastic method is provided in ref 13. In the simulations performed in the present work, the relative stabilities of alternative complexes and the energies of the elementary reactions obtained for the real catalyst were used as data for these simulations.

Acknowledgment. The authors thank The University of Akron for financial support of the experimental work. R.A.S. acknowledges the support of the Eastman Chemical Co. for a graduate scholarship. J.C. thanks the donors of the Petroleum Research Fund, administered by the American Chemical Society, for partial stipend support. Z.F., J.B.P.S., and T.Z. acknowledge the financial support of the Natural Sciences and Engineering Research Council of Canada. A.N. and P.L.R. wish to thank the Kresge Foundation and donors to the Kresge Challenge Program at The University of Akron for funds used to purchase the NMR instrument used in this work. The authors thank Mr. Douglas Medvetz and Prof. Wiley J. Youngs of the Department of Chemistry at The University of Akron for collection of the X-ray crystallographic data, structure solution and refinement of complex **2**.

Supporting Information Available: Tables of crystallographic data, atomic coordinates and isotropic thermal parameters, bond lengths and angles, anisotropic thermal parameters and H atom coordinates and isotropic thermal parameters for complex **2** and figures showing ^1H and ^{13}C NMR spectra of oligomeric PE prepared using complex **2** and a ball and stick diagram of **2**. This material is available free of charge via the Internet at http://pubs.acs.org.

References and Notes

(1) (a) Stadler, F. J.; Piel, C.; Klimke, K.; Kaschta, J.; Parkinson, M.; Wilhelm, M.; Kaminsky, W.; Muenstedt, H. *Macromolecules* **2006**, *39*, 1474−1482. (b) Arikan, B.; Kaminsky, W. *Des. Monomers Polym.* **2005**, *8*, 589−600. (c) Li, H.; Stern, C. L.; Marks, T. J. *Macromolecules* **2005**, *38*, 9015−9027. (d) Bianchini, C.; Frediani, M.; Giambastiani, G.; Kaminsky, W.; Meli, A.; Passaglia, E. *Macromol. Rapid Commun.* **2005**, *26*, 1218−1223. (e) Wang, J.; Li, H.; Guo, N.; Li, L.; Stern, C. L.; Marks, T. J. *Organometallics* **2004**, *23*, 5112−5114. (f) Sworen, J. C.; Smith, J. A.; Berg, J. M.; Wagener, K. B. *J. Am. Chem. Soc.* **2004**, *126*, 11238−11246. (g) Capacchione, C.; Proto, A.; Okuda, J. *J. Polym. Sci., Part A: Polym. Chem.* **2004**, *42*, 2815−2822. (h) Sperber, O.; Kaminsky, W. *Macromolecules* **2003**, *36*, 9014−9019. (i) Heinicke, J.; Koehler, M.; Peulecke, N.; He, M.; Kindermann, M. K.; Keim, W.; Fink, G. *Chem.−Eur. J.* **2003**, *9*, 6093−6107. (j) Kasi, R. M.; Coughlin, E. B. *Macromolecules* **2003**, *36*, 6300−6304. (k) Kunrath, F. A.; Mota, F. F.; Casagrande, O. L., Jr.; Mauler, R. S.; de Souza, R. F. *Macromol. Chem. Phys.* **2002**, *203*, 2407−2411. (l) Komon, Z. J. A.; Diamond, G. M.; Leclerc, M. K.; Murphy, V.; Okazaki, M.; Bazan, G. C. *J. Am. Chem. Soc.* **2002**, *124*, 15280−15285. (m) Li, L.; Metz, M. V.; Li, H.; Chen, M.-C.; Marks, T. J.; Liable-Sands, L.; Rheingold, A. L. *J. Am. Chem. Soc.* **2002**, *124*, 12725−12741. (n) Schroeder, D. L.; Keim, W.; Zuideveld, M. A.; Mecking, S. *Macromolecules* **2002**, *35*, 6071−6073. (o) Galland, G. B.; Quijada, R.; Rojas, R.; Bazan, G.; Komon, Z. J. A. *Macromolecules* **2002**, *35*, 339−345. (p) Guan, Z. *Chem.−Eur. J.* **2002**, *8*, 3086−3092. (q) Coates, G. W.; Hustad, P. D.; Reinartz, S. *Angew. Chem., Int. Ed.* **2002**, *41*, 2236−2257. (r) Beigzadeh, D.; Soares, J. B. P.; Duever, T. A. *Macromol. Symp.* **2001**, *173*, 179−194. (s) Komon, Z. J. A.; Bazan, G. C. *Macromol. Rapid Commun.* **2001**, *22*, 467−478. (t) Gottfried, A. C.; Brookhart, M. *Macromolecules* **2001**, *34*, 1140−1142. (u) Walter, P.; Trinkle, S.; Suhm, J.; Mader, D.; Friedrich, C.; Mulhaupt, R. *Macromol. Chem. Phys.* **2000**, *201*, 604−612. (v) Hadjichristidis, N.; Xenidou, M.; Iatrou, H.; Pitsikalis, M.; Poulos, Y.; Avgeropoulos, A.; Sioula, S.; Paraskeva, S.; Velis, G.; Lohse, D. J.; Schulz, D. N.; Fetters, L. J.; Wright, P. J.; Mendelson, R. A.; Garcia-Franco, C. A.; Sun, T.; Ruff, C. J. *Macromolecules* **2000**, *33*, 2424−2436. (w) Held, A.; Mecking, S. *Chem.−Eur. J.* **2000**, *6*, 4623−4629. (x) Simon, L. C.; Mauler, R. S.; De Souza, R. F. *J. Polym. Sci., Part A: Polym. Chem.* **1999**, *37*, 4656−4663. (y) Mecking, S. *Macromol. Rapid Commun.* **1999**, *20*, 139−143.

(2) (a) Malmberg, A.; Kokko, E.; Lehmus, P.; Loefgren, B.; Seppaelae, J. V. *Macromolecules* **1998**, *31*, 8448−8454. (b) Harrison, D.; Coulter, I. M.; Wang, S.; Nistala, S.; Kuntz, B. A.; Pigeon, M.; Tian, J.; Collins, S. *J. Mol. Catal. A: Chem.* **1998**, *128*, 65−77. (b) Lai, S.-Y.; Wilson, J. R.; Knight, G. W.; Stevens, J. C.; Chum, P.-W. S. PCT Int. Appl. WO 9607680, 1996. (c) Stevens, J. C. *Stud. Surf. Sci. Catal.* **1994**, *89*, 277−84. (d) Lai, S.-Y.; Wilson, J. R.; Knight, G. W.; Stevens, J. C. U.S. Patent 5,278,272, 1994. (e) Lai, S.-Y.; Wilson, J. R.; Knight, G. W.; Stevens, J. C. PCT Int. Appl. WO 9308221, 1993. (f) Stevens, J. C.; Timmers, F. J.; Wilson, D. R.; Schmidt, G. F.; Nickias, P. N.; Rosen, R. K.; Knight, G. W.; Lai, S.-Y. Eur. Pat. Appl. EP 416815, 1991.

(3) (a) Simon, L. C.; Soares, J. B. P. *Ind. Eng. Chem. Res.* **2005**, *44*, 2461−2468. (b) Soares, J. B. P. *Macromol. Mater. Eng.* **2004**, *289*, 70−87. (c) Arjunan, P.; Dekmezian, A. H.; Markel, E. J.; Weng, W.; Garcia-Franco, C.; Jiang, P.; Soares, J. B. P.; Bonchev, D. *PMSE Prepr.* **2004**, *91*, 47−48. (d) Nele, M.; Soares, J. B. P. *Macromol. Theory Simul.* **2002**, *11*, 939−943. (e) Simon, L. C.; Soares, J. B. P. *Macromol. Theory Simul.* **2002**, *11*, 222−232. (f) Soares, J. B. P. *Macromol. Theory Simul.* **2002**, *11*, 184−198. (g) Soares, J. B. P. *Chem. Eng. Sci.* **2001**, *56*, 4131−4153. (h) Soares, J. B. P.; Penlidis, A. *Metallocene-Based Polyolefins* **2000**, *2*, 237−267. (i) Beigzadeh, D.; Soares, J. B. P.; Duever, T. A.; Hamielec, A. E. *Polym. React. Eng.* **1999**, *7*, 195−205. (j) Beigzadeh, D.; Soares, J. B. P.; Hamielec, A. E. *J. Appl. Polym. Sci.* **1999**, *71*, 1753−1770. (k) Beigzadeh, D.; Soares, J. B. P.; Hamielec, A. E. *Polym. React. Eng.* **1997**, *5*, 141−180.

(4) (a) Liu, W.; Brookhart, M. *Organometallics* **2004**, *23*, 6099−6107. (b) Leatherman, M. D.; Svejda, S. A.; Johnson, L. K.; Brookhart, M. *J. Am. Chem. Soc.* **2003**, *125*, 3068−3081. (b) Gottfried, A. C.; Brookhart, M. *Macromolecules* **2003**, *36*, 3085−3100. (c) Shultz, L. H.; Tempel, D. J.; Brookhart, M. *J. Am. Chem. Soc.* **2001**, *123*, 11539−11555. (d) Shultz, L. H.; Brookhart, M. *Organometallics* **2001**, *20*, 3975−3982. (e) Gottfried, A. C.; Brookhart, M. *Macromolecules* **2001**, *34*, 1140−1143. (e) Tempel, D. J.; Johnson, L. K.; Huff, R. L.; White, P. S.; Brookhart, M. *J. Am. Chem. Soc.* **2000**, *122*, 6686−6700. (f) Gates, D. P.; Svejda, S. A.; Onate, E.; Killian, C. M.; Johnson, L. K.; White, P. S.; Brookhart, M. *Macromolecules* **2000**, *33*, 2320−2334. (g) Svejda, S. A.; Johnson, L. K.; Brookhart, M. *J. Am. Chem. Soc.* **1999**, *121*, 10634−10635. (h) Tanner, M. J.; Brookhart, M.; DeSimone, J. M. *J. Am. Chem. Soc.* **1995**, *119*, 7617−7618. (i) Killian, C. M.; Tempel, D. J.; Johnson, L. K.; Brookhart, M. *J. Am. Chem. Soc.* **1996**, *118*, 11664−11665. (j) Johnson, L. K.; Killian, C. M.; Brookhart, M. *J. Am. Chem. Soc.* **1995**, *117*, 6414−6415.

(5) (a) Plentz-Meneghetti, S.; Kress, J.; Peruch, F.; Lapp, A.; Duval, M.; Muller, R.; Lutz, P. J. *Polymer* **2005**, *46*, 8913−8925. (b) Patil, R.; Colby, R. H.; Read, D. J.; Chen, G.; Guan, Z. *Macromolecules* **2005**, *38*, 10571−10579. (c) Ye, Z.; Al-Obaidi, F.; Zhu, S. *Macromol. Chem. Phys.* **2004**, *205*, 897−906. (d) Guan, Z. *J. Polym. Sci., Part A: Polym, Chem.* **2003**, *41*, 3680−3692. (e) Guan, Z.; Cotts, P. M. *Polym. Mater. Sci. Eng.* **2001**, *84*, 382−383. (f) Cotts, P. M.; Guan, Z.; McCord, E.; McLain, S. *Macromolecules* **2000**, *33*, 6945−6952. (g) Guan, Z.; Cotts, P. M.; McCord, E. F.; McLain, S. J. *Science* **1999**, *283*, 2059−2062.

(6) Odian, G. *Principles of Polymerization*, 3rd ed.; John Wiley and Sons, Inc.: New York, 1991; pp 304−306. However see ref 1c.

(7) For a recent example, using an unhindered Ni diimine catalyst, see: Zou, H.; Zhu, F. M.; Wu, Q.; Ai, J. Y.; Lin, S. A. *J. Polym. Sci., Part A: Polym. Chem.* **2005**, *43*, 1325−1330.

(8) Keim, W.; Appel, R.; Storeck, A.; Kruger, C.; Goddard, R. *Angew. Chem., Int. Ed. Engl.* **1981**, *20*, 116−117.

(9) (a) Möhring, V. M.; Fink, G. *Angew. Chem.* **1985**, *97*, 982−984. (b) Fink, G.; Möhring, V. M. Patent Application EP 01/94456 A2, 1986. (c) Schubbe, R.; Angermund, K.; Fink, G.; Goddard, R. *Macromol. Chem. Phys.* **1995**, *196*, 467−478.

(10) (a) Yano, A.; Hasegawa, S.; Yamada, S. *Kobunshi Ronbunshu* **2002**, *59*, 377−381; cf. *Chem. Abstr.* **2002**, *137*, 201636. (b) Yano, A.; Yamada, S.; Yamada, K. U.S. Patent 5,324,799, 1994; Cont.-in-part of U.S. Ser. No. 662,167, abandoned. (c) Yano, A.; Yamada, S.; Yamada, K. Eur. Pat. Appl. 0446013, 1991. (d) Yano, A.; Naito, Y.; Yamada, K.; Ohtsuru, M. Eur. Pat. Appl. 0381495, 1990.

(11) (a) Stapleton, R. A.; Chai, J.; Taylor, N. J.; Collins, S. *Organometallics* **2006**, *25*, 2514−2524. (b) Stapleton, R. A.; Nuamthanom, A.; Rinaldi, P. L.; Taylor, N. J.; Collins, S. *Polym. Prepr.* **2004**, *45*, 93−94.

(12) (a) Soares, J. B. P.; Simon, L. C.; De Souza, R. F. *Polym. Reaction Eng.* **2001**, *9*, 199−223. (b) Simon, L. C.; Williams, C. P.; Soares, J. B. P.; de Souza, R. F. *Chem. Eng. Sci.* **2001**, *56*, 4181−4190. (c) Simon, L. C.; Soares, J. B. P.; De Souza, R. F. *AIChE J.* **2000**, *46*, 1234−1240.

(13) (a) Michalak, A.; Ziegler, T. *Organometallics* **2003**, *22*, 2069−2079. (b) Michalak, A.; Ziegler, T. *Macromolecules* **2003**, *36*, 928−933. (c) Michalak, A.; Ziegler, T. *J. Am. Chem. Soc.* **2002**, *124*, 7519−7528. (d) Michalak, A.; Ziegler, T. *J. Am. Chem. Soc.* **2001**, *123*, 12266−12278. (e) Michalak, A.; Ziegler, T. *Organometallics* **2000**, *19*, 1850−1858. (f) Woo, T. K.; Bloechl, P. E.; Ziegler, T. *J. Phys. Chem. A* **2000**, *104*, 121−129. (g) Michalak, A.; Ziegler, T. *Organometallics* **1999**, *18*, 3998−4004. (h) Deng, L.; Woo, T. K.; Cavallo, L.; Margl, P. M.; Ziegler, T. *J. Am. Chem. Soc.* **1995**, *119*, 6177−6186. (i) Deng, L.; Margl, P.; Ziegler, T. *J. Am. Chem. Soc.* **1995**, *119*, 1094−1100.

(14) (a) Jolly, P. W. in *Comprehensive Organometallic Chemistry*; Wilkinson, G., Stone, F. G. A., Abel, E., Eds.; Pergamon: Oxford, U.K., 1982; Vol. 6, pp 145−182. (b) Henc, B.; Jolly, P. W.; Salz, R.; Stobbe, S.; Wilke, G.; Benn, R.; Mynott, R.; Seevogel, K.; Goddard, R.; Krueger, C. *J. Organomet. Chem.* **1980**, *191*, 449−475. (c) Jolly, P. W.; Wilke, G. *The Organic Chemistry of Nickel*; Academic: New York, 1974; Vol. 1. (d) Wilke, G.; Bogdanovic, B.; Hardt, P.; Heimbach, P.; Keim, W.; Kroner, M.; Oberkirch, W.; Tanaka, K.; Walter, D. *Angew. Chem., Int. Ed. Engl.* **1966**, *5*, 151−164. (e) Walter, D.; Wilke, G. *Angew. Chem., Int. Ed. Engl.* **1966**, *5*, 897−898. (f) Wilke, G.; Bogdanovic, B. *Angew. Chem.* **1961**, *73*, 756.

(15) Boennemann, H.; Bogdanovic, B.; Wilke, G. *Angew. Chem., Int. Ed. Engl.* **1965**, *6*, 804.

(16) (a) Piel, C.; Stadler, F. J.; Kaschta, J.; Rulhoff, S.; Muenstedt, H.; Kaminsky, W. *Macromol. Chem. Phys.* **2006**, *207*, 26−38. (b) Wang, W.-J.; Kharchenko, S.; Migler, K.; Zhu, S. *Polymer* **2004**, *45*, 6495−6505. (b) Yu, Y.; DesLauriers, P. J.; Rohlfing, D. C. *Polymer* **2005**, *46*, 5165−5182. (c) Cotts, P. M. *Polym. Prepr.* **2002**, *43*, 297−298. (d) Cotts, P. M.; Guan, Z.; McCord, E.; McLain, S. *Macromolecules* **2000**, *33*, 6945−6952.

(17) It should be noted that most metallocene catalyzed HDPE contains sparse levels of long chain branching, depending on catalyst and conditions.[1−2] Therefore it can be concluded that the higher MW PE sample prepared using the Keim catalyst must have higher levels of LCB than the "linear" PE standard used.

(18) (a) Guangxue Xu, G.; Cheng, G. *Macromolecules* **2001**, *34*, 2040−2047. (b) McLain, S. J.; McCord, E. F.; Johnson, L. K.; Ittel, S. D.; Nelwson, L. T. J.; Arthur, S. D.; Halfhill, M. J.; Teasley, M. F. *Polym. Prepr.* **1997**, *38*, 772−773.

(19) Collins, S.; Ziegler, T. Manuscript in preparation.

(20) Flisak, Z.; Ziegler, T. *Macromolecules* **2005**, *38*, 9865−72.

(21) Press, W. H.; Teukolsky, S. A.; Vetterling, W. T.; Flannery, B. P. *Numerical recipes in Fortran 77. The Art of Scientific Computing*, 2nd ed.; Press Syndicate of the University of Cambridge: Cambridge, U.K., New York, and Melbourne, Australia, 1992.

(22) Indeed, when entropy is included and dissolved [C_2H_4] (as opposed to *P*) is used as the variable, the simulations predict extensive (but unproductive) chain-walking compared to insertion. The use of eq 6 to calculate reaction probabilities under such conditions is not valid; Curtin Hammett conditions would apply to the various Ni−R present. In this case, it is the relative stability of the π complexes and the insertion barriers that will dictate the branching distribution.

(23) Chen, Z.; Gospodinov, I.; Escobedo, F. A. *Macromol. Theory Simul.* **2002**, *11*, 1022−1344.

(24) (a) Reinking, M. K.; Orf, G.; Mcfaddin, D. *J. Polym. Sci., Part A: Polym. Chem.* **1998**, *36*, 2889−2898. (b) Resconi, L.; Piemontesi, F.; Franciscono, G.; Abis, L.; Fiorani, T. *J. Am. Chem. Soc.* **1992**, *114*, 1025−32.

(25) The metallocene system studied[24b] was selective for C−H activation of 4-methyl-1-pentene at the fifth C atom removed from the metal− by definition this is the longest branch that could form from this monomer. Preliminary DFT calculations suggest that the inter- or intramolecular C−H activation process has a low barrier ($\sim$10 kcal mol^{-1}) but with a very unfavorable pre-equilibrium in forming the relevant agostic alkyl from the most stable β-agostic structure.

(26) Pangborn, A. B.; Giardello, M. A.; Grubbs, R. H.; Rosen, R. K.; Timmers, F. J. *Organometallics* **1996**, *15*, 1518−1520.

(27) Hidai, M.; Kashiwagi, T.; Ikeuchi, T.; Uchida, Y. *J. Organomet. Chem.* **1971**, *30*, 279−282.

(28) Krysan, D. J.; Mackenzie, P. B. *J. Org. Chem.* **1990**, *55*, 4229−4230.

(29) Birkofer, L.; Wegner, P.; Merritt, R. F.; Emmons, W. D. *Org. Synth.* **1970**, *50*, 107−110.

(30) (a) Niecke, E.; Oberdorfer, R.; Bajorat, V. *Synth. Met. Organomet. Inorg. Chem.* **1996**, *3*, 36−37. (b) Niecke, E.; Oberdorfer, R.; Bajorat, V. *Synth. Met. Organomet. Inorg. Chem.* **1996**, *3*, 84−85.

(31) (a) Romanenko, V. D.; Shul'gin, V. F.; Skopenko, V. V.; Markovskii, L. N. *Zh. Obshch. Khim.* **1985**, *55*, 538−43. (b) Romanenko, V. D.; Shul'gin, V. F.; Brusilovets, A. I.; Skopenko, V. V.; Markovskii, L. N. *Zh. Obshch. Khim.* **1983**, *53*, 1428−9.

(32) (a) Becke, A. *Phys. Rev. A* **1988**, *38*, 3098. (b) Perdew, J. P. *Phys. Rev. B* **1986**, *34*, 7406. (c) Perdew, J. P. *Phys. Rev. B* **1986**, *33*, 8822.

(33) (a) Te Velde, G.; Bickelhaupt, F. M.; Baerends, E. J.; Fonseca Guerra, C.; Van Gisbergen, S. J. A.; Snijders, J. G.; Ziegler, T *J. Comput. Chem.* **2001**, *22*, 931, and references therein. (b) Te, Velde, G.; Baerends, E. J. *J. Comput. Phys.* **1992**, *99*, 84. (c) Boerrigter, P. M.; te Velde, G.; Baerends, E. J. *Int. J. Quantum Chem.* **1988**, *33*, 87. (d) Versluis, L.; Ziegler, T. *J. Chem. Phys.* **1988**, *88*, 322. (e) Baerends, E. J.; Ellis, D. E.; Ros, P. *Chem. Phys.* **1973**, *2*, 41.

(34) Fonesca Geurra, C.; Visser, O.; Snijders, J. G.; te Velde, G.; Baerends, E. J. In *Methods and Techniques in Computational Chemistry METACC-95*; Clementi, E., Corongiu, G., Eds.; STEF: Cagliari, Italy, 1995.

(35) Snijders, J. G.; Baerends, E. J.; Vernoijs, P. *At. Nucl. Data Tables* **1982**, *26*, 483.

(36) Woo, T. K.; Cavallo, L.; Ziegler, T. *Theor. Chem. Acc.* **1998**, *100*, 307.

(37) Clark, M.; Cramer, R. D., III; van Opdenbosch, N. *J. Comput. Chem.* **1989**, *10*, 982.

(38) Rappé, A. K.; Casewit, C. J.; Colwell, K. S.; Goddard, W. A., III; Skiff, W. M. *J. Am. Chem. Soc.* **1992**, *114*, 10024.

MA062332F